Available online at www.sciencedirect.com

Manufacturing Letters

Manufacturing Letters 33 (2022) 355–364

50th SME North American Manufacturing Research Conference (NAMRC 50, 2022)

Dynamic force and stability prediction for milling using feed rate scheduling software and time-domain simulation

Jose Nazario[a], Timothy No[a], Michael Gomez[b], Greg Corson[a], and Tony Schmitz[a,b]*

[a]*University of Tennessee, Knoxville, Knoxville, TN 37966, USA*
[b]*Oak Ridge National Laboratory, Manufacturing Demonstration Facility, Knoxville, TN 37932, USA*

* Corresponding author. Tel.: +1-865-974-6141. *E-mail address:* tony.schmitz@utk.edu

Abstract

This paper describes: 1) the use of feed rate scheduling software to predict the radial depth of cut variation for three-axis milling toolpaths and; 2) the use of the radial depth profile in a time-domain simulation to predict dynamic cutting forces. The time-domain simulation, which also includes the tool tip frequency response functions and force model (which relates the cutting force components to the chip geometry) as inputs, enables dynamic force profiles to be predicted and parameter combinations that cause chatter to be identified. A ramp geometry is selected that provides constantly varying radial depth and force predictions are completed at multiple axial depths for comparison to measured forces. Both stable and unstable (chatter) milling conditions were observed with good agreement between time-domain simulation and measurement results. The value of combining the feed rate scheduling software and time-domain simulation is demonstrated.

Keywords: Milling; dynamics; feed rate scheduling; simulation

1. Introduction

Predictive models are required to select optimal milling parameters, including axial and radial depths of cut, spindle speed, and feed per tooth, at the process planning stage. The intent is to select parameters that enable first part correct performance to avoid costly and time-consuming trial and error parameter identification. This first part correct performance requires that chatter, or self-excited vibration, does not occur and acceptable geometric accuracy and surface finish are achieved. Available predictive models for milling dynamics include: analytical, frequency-domain solutions for milling stability [1-5] and surface location error (SLE, forced vibration which leads to part geometry errors) [6-8]; time-domain simulation for milling force and vibration, which can be used to assess stability and SLE [9-16]; and semi-discretization methods for milling force and vibration, which can again be used to assess stability and SLE [17-20]. The purpose of these models is to relate the milling parameters, process dynamics, and milling performance in a mathematical framework.

Another class of predictive models relates the milling parameters to the cutting and non-cutting times given the part geometry. These computer-aided manufacturing (CAM) models use the peak cutting force, which depends on the part geometry, computer numerically controlled (CNC) tool path, and milling parameters, to modify the cutting and non-cutting times by updating the instantaneous feed rate along the tool path. The outcome is optimized cutting and non-cutting times for maximum productivity. This feed rate scheduling approach simultaneously consider the acceleration (and potentially jerk) limits of the CNC machining center drives [21-22], spline tool paths [22], and cutting force [23]. Commercial feed rate scheduling software is gaining acceptance in industrial applications to optimize CNC part programs.

To date, however, these two predictive capabilities have remained separate. Machining dynamics models do not

typically include the time-dependent cutting conditions imposed by CNC tool paths. They tend to focus on, for example, a fixed radial depth to determine stable combinations of spindle speed and axial depth in the graphical form of a stability map or the variation in SLE with spindle speed for a selected combination of radial depth, axial depth, and feed per tooth; both cases depend on the selected workpiece material. Feed rate scheduling solutions, on the other hand, do consider the variable cutting conditions for arbitrary three-axis and five-axis tool paths, but do not include the effects of relative vibration between the cutting tool and workpiece on the process stability and SLE. This relative vibration occurs because the tool and workpiece are not rigid and a complete solution requires more than geometry.

The purpose of this paper is to, for the first time, combine time-domain milling simulation and feed rate scheduling software to predict the dynamic cutting force components for a tool path with variable radial depth of cut. Both stable and unstable (chatter) milling conditions are considered. The time-domain simulation inputs include the tool tip frequency response function (FRF, which describes the vibration behavior), cutting force model, and instantaneous radial depth of cut. The latter is obtained from the feed rate scheduling software Production Module provided by Third Wave Systems [24].

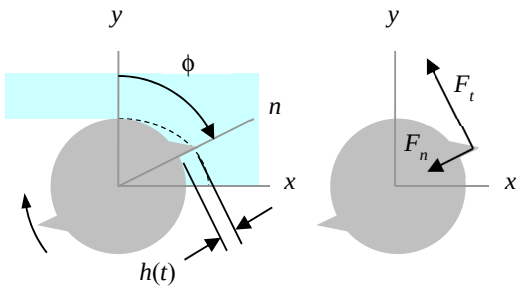

Fig. 1. Milling model (up milling is shown, but the model is generic to up or down milling.

2. Time-domain simulation

Time-domain simulation provides numerical solution of the coupled, second-order, time-delay differential equations of motion for milling in small time steps [15]. It is well suited to incorporating the inherent complexities of milling dynamics, including tool geometries and the nonlinearity that occurs if the tooth leaves the cut due to large amplitude vibrations. The time-domain simulation used in this study predicts the time-dependent cutting force and vibration behavior by the following steps:

1. The instantaneous chip thickness, $h(t)$, is determined using the commanded chip thickness, instantaneous radial depth of cut, which depends on the CNC tool path, runout of the cutter teeth, and vibration of the current and previous teeth at the selected tooth angle for the current axial slice (discretized axial depth).
2. The cutting force components in the tangential, t, and normal, n, directions are calculated at each axial slice using the cutting force coefficients and process damping coefficients:

$$F_t(t) = k_{tc} b h(t) + k_{te} b - C_t \frac{b}{V} \dot{n} \quad (1)$$

$$F_n(t) = k_{nc} b h(t) + k_{ne} b - C_n \frac{b}{V} \dot{n} \quad (2)$$

where b is the axial slice width; the cutting force coefficients are identified by the subscripts t or n for direction and c or e for cutting or edge; the process damping coefficients are identified by the subscripts t or n for direction; V is the cutting speed; and $\dot{n}$ is the instantaneous tool vibration velocity in the normal (radial) direction. These forces are then summed over all axial slices engaged in the cut for the instantaneous radial depth.
3. The summed force components are used to find the new displacements by numerical (modified Euler) integration of the second-order delay differential equations of motion in the x (feed) and y directions:

$$m_x \ddot{x} + c_x \dot{x} + k_x x = F_t(t)\cos\phi + F_n(t)\sin\phi \quad (3)$$

$$m_y \ddot{y} + c_y \dot{y} + k_y y = F_t(t)\sin\phi - F_n(t)\cos\phi \quad (4)$$

where m is the tool tip modal mass, c is the modal viscous damping coefficient, k is the modal stiffness, and ϕ is the tool rotation angle; see Fig. 1. The subscripts (x or y) identify the direction. While these equations include only a single degree of freedom in each direction, multiple degrees-of-freedom in each direction can be accommodated by summing the modal contributions individually.
4. The tool rotation angle is incremented, and the process is repeated.

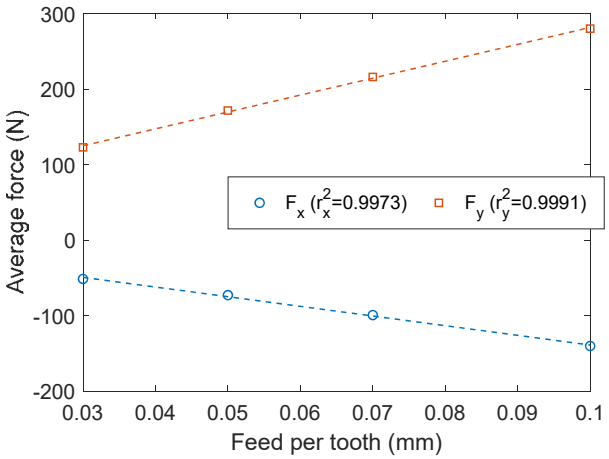

Fig. 2. Average values (symbols) and linear regressions (dashed lines) for x and y force components. The coefficient of determination (r^2) for both linear fits is included in the legend.

3. Data collection

3.1. Force model

The four cutting force coefficients in Eqs. 1 and 2 were identified experimentally using the average force, linear regression approach [15]. Down milling tests were completed for: 3.18 mm radial depth (25% radial immersion), 9.0 mm axial depth, 7000 rpm spindle speed, and four feed per tooth values {0.03, 0.05, 0.07, 0.10} mm with the 6061-T6 extruded aluminum bar stock workpiece mounted on a Kistler 9257B cutting force dynamometer. The mean force in the *x* (feed) and *y* directions was plotted versus the commanded feed per tooth values and a linear regression was completed to identify the slope and intercept values; see Fig. 2. These slope and intercept values were then used to calculate the cutting force coefficients [4].

Process damping is described as energy dissipation due to interference between the cutting tool clearance face and machined surface during relative vibrations between the tool and workpiece [25-34]. Tyler and Schmitz [33-34] performed cutting tests to determine process damping coefficients for various workpiece materials. These results were used for this study, where the tangential and normal direction coefficients were assumed to be identical. The cutting force coefficients and process damping coefficients are listed in Table 1.

Table 1. Force model coefficient values.

Coefficient	Value	Units
k_{tc}	867×10^6	N/m^2
k_{nc}	332×10^6	N/m^2
k_{te}	6.7×10^3	N/m
k_{ne}	7.8×10^3	N/m
C_t	1.4×10^5	N/m
C_n	1.4×10^5	N/m

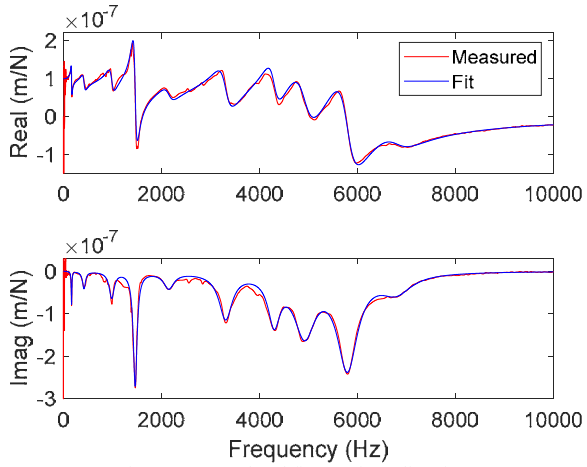

Fig. 3. Measured and fit FRF for *x* direction.

3.2. Tool tip FRFs

The tool tip FRF was measured by tap testing, where an instrumented hammer is used to excite the tool tip with a known force and the corresponding vibration response is measured using a low-mass accelerometer [15]. These time responses are converted to the frequency domain using the Fourier transform and the ratio of the response to the force is calculated. The measurement was performed in both the *x* and *y* directions using MLI's TXF software and data acquisition. The PCB Piezotronics hammer was model number 086C04 and the accelerometer was model number 352C23. The 12.7 mm diameter, four helical flute, square carbide endmill was produced by HTC and the model number was 1.001-.500-1.375. A Maritool ER 32 collet holder (model number ER32-2.35) was used to clamp the tool and the spindle interface was CAT 40 for the Haas VF-4 three-axis CNC milling machine.

The tool tip FRFs for the *x* and *y* directions are displayed in Figs. 3 and 4. A modal fit was performed for each FRF so the associated modal mass, damping coefficient, and stiffness values could be used in the time domain simulation. These values are provided in Table 2.

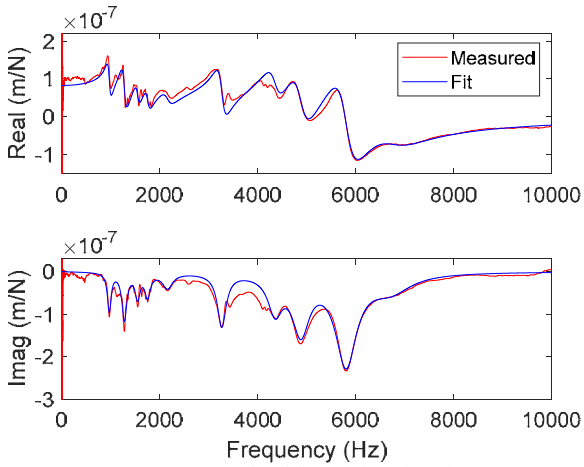

Fig. 4. Measured and fit FRF for *y* direction.

Table 2. Modal parameters from fits to measured tool tip FRFs.

m (kg)	*k* (N/m)	*c* (N-s/m)
	x direction	
123	1.37×10^8	1.24×10^4
3.47	1.34×10^8	2.67×10^3
0.70	5.96×10^7	4.07×10^2
0.22	9.55×10^7	4.52×10^2
0.19	1.37×10^8	3.46×10^2
0.07	6.83×10^7	2.33×10^2
0.04	5.26×10^7	1.25×10^2
0.11	2.00×10^8	5.35×10^2
1.25	2.30×10^8	2.00×10^3
20.8	1.47×10^8	9.39×10^3
	y direction	
3.19	1.19×10^8	1.83×10^3
1.48	9.57×10^7	1.14×10^3
2.45	2.32×10^8	1.83×10^3
1.99	2.42×10^8	1.69×10^3
1.32	2.43×10^8	2.08×10^3
0.29	1.23×10^8	3.95×10^2
0.20	1.50×10^8	4.38×10^2
0.09	8.71×10^7	2.46×10^2
0.04	5.27×10^7	1.30×10^2
0.09	1.57×10^8	5.71×10^2

4. Part geometry

To provide a continuously variable radial depth of cut with a fixed axial depth, the part geometry displayed in Fig. 5 was selected. The combination of varying radial depth with fixed axial depth mimics traditional three-axis, 2.5D CNC machining toolpaths, where the material is removed with *x*-*y* planar toolpaths that implement the user-selected stepover (radial depth) and advance the stepdown in the *z* direction (axial depth) between each planar toolpath. The Fig. 5 geometry was machined multiple times using a different (constant) axial depth between tests to advance from stable (low axial depth) to unstable, or chatter, (high axial depth) cutting conditions. The workpiece material was 6061-T6 aluminum in all cases.

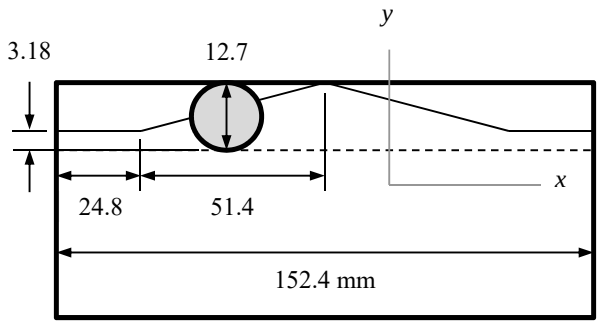

Fig. 5. Part geometry. The ramp geometry continuously varied the radial depth from 3.18 mm (25% radial immersion) to 12.7 mm (slotting) and back for the left to right down milling operation. The axial depth (into the page) was constant and was varied between tests. The 12.7 mm diameter endmill is represented by the circle.

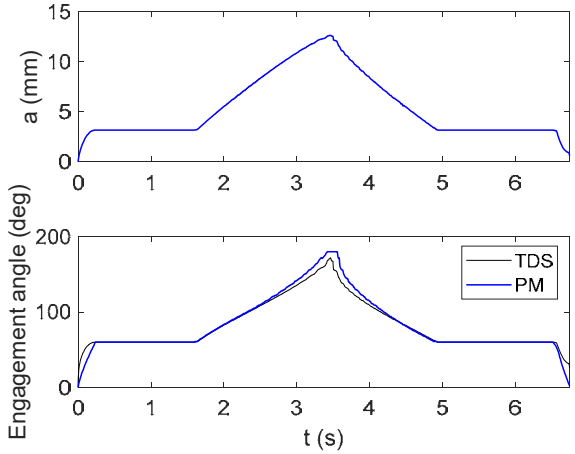

Fig. 6. (Top) Variation in instantaneous radial depth of cut, *a*, with time for the part geometry shown in Fig. 5. (Bottom) Variation in engagement angle (i.e., tooth entry to exit angle for the down milling operation) with time.

5. Feed rate scheduling software output

Given the CAM toolpath and machining parameters, Production Module calculates the position-dependent radial depth of cut, angle of engagement between the rotating endmill and workpiece, and peak force values. For the part geometry shown in Fig. 5, the variation in radial depth of cut with cutting time is displayed in the top panel of Fig. 6. The constant radial depth of 3.18 mm is observed at the beginning and end of the toolpath. The radial depth increases from 3.18 mm (25% radial immersion) to 12.7 mm (slotting) at the center of the cut. The variation in angle of engagement is shown in the bottom panel of Fig. 6. The angle is 60 deg for the 25% radial immersion portion of the toolpath and increases to 180 deg for the slotting condition in the middle of the toolpath. For comparison, the angle of engagement calculated by both Production Module (PM) and time-domain simulation (TDS) are displayed. Good agreement is observed.

The variation in radial depth/angle of engagement seen in Fig. 6 can cause the milling performance to transition from stable to unstable (chatter) behavior. This dependence of the milling performance on the axial/radial depth of cut, machining parameters, structural dynamics, and workpiece material motivates the combination of the feed rate scheduling software and time-domain simulation.

6. Cutting force measurements and predictions

Force measurements and predictions were completed for two workpiece geometries. First, the radial depth of cut was held constant and the measurement/prediction comparison was performed for variation axial depth-radial depth combinations to confirm the accuracy of the force model (Eqs. 1 and 2 with Table 1 coefficients). Second, the ramp profile was machined at multiple axial depths of cut and the measurement/prediction comparison was completed. For both geometries, the programmed toolpath was opened using Production Module and the radial depth of cut profile was predicted. This variation in radial depth with time in the toolpath served as a key input to the time-domain simulation. The peak force profiles were also predicted by Production Module and compared to the measurement and time-domain simulation forces.

6.1. Constant radial depth

The setup described in Section 3.1 was used to machine a 6061-T6 aluminum workpiece bolted to a Kistler 9257B cutting force dynamometer. The radial depths of cut varied from 3.18 mm (25% radial immersion) to 12.7 mm (100% radial immersion) and the axial depths were varied from 3 mm to 12 mm. The spindle speed was 7000 rpm and the feed per tooth was 0.05 mm in all cases. Flood coolant was applied to evacuate chips.

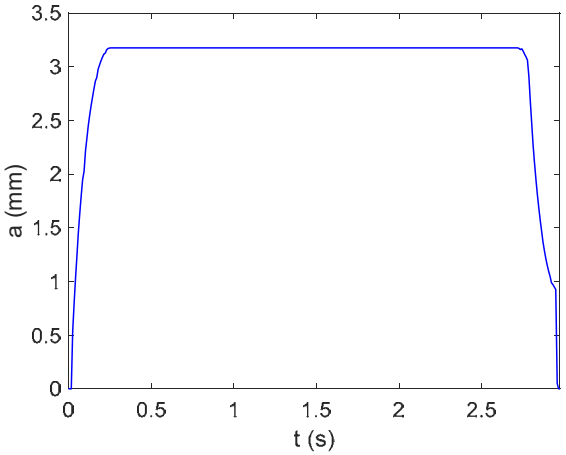

Fig. 7. Production Module radial depth of cut, *a*, for 25% radial immersion down milling operation.

Figure 7 shows the radial depth of cut profile for a 25% radial immersion down milling operation. It is seen that the depth is 3.18 mm except for the cut entry and exit, where it increases and decreases with time. The Production Module peak force profiles are displayed in Fig. 8. The axial depth for this case is 5 mm. The radial depth variation was input to the time-domain simulation, as well as the tool tip FRFs and force model, and the simulation was used to predict the dynamic cutting forces in the x (feed) and y directions. Figure 9 shows the time-dependent x and y direction force components, Fig. 10 displays the resultant force (vector sum of F_x and F_y), Fig. 11 shows the force variation during the cut entry (first 0.1 s), and Fig. 12 gives the steady-state force (1.4 s to 1.5 s). In all cases, the measured force was inverse filtered to remove the effects of the dynamometer dynamics; see Appendix A.

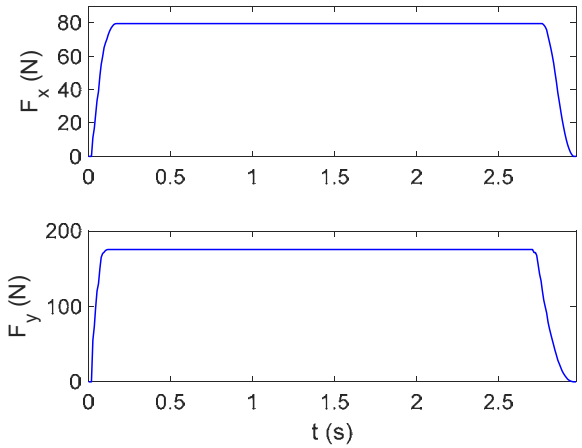

Fig. 8. (Top) Production Module peak force in the x direction, F_x. (Bottom) Peak force in the y direction, F_y. The radial depth is provided by Fig. 7 and the axial depth is 5 mm.

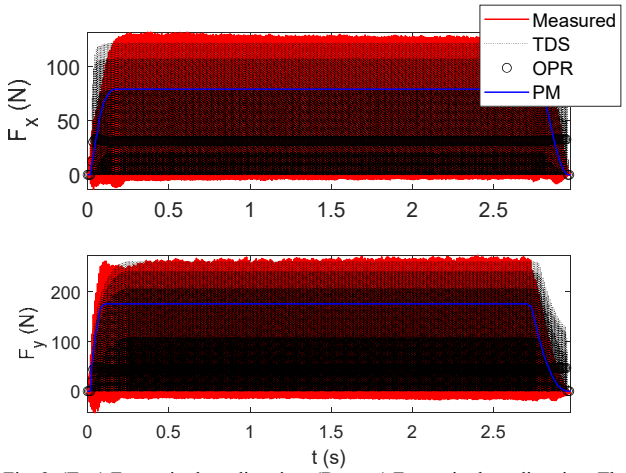

Fig. 9. (Top) Forces in the x direction. (Bottom) Forces in the y direction. The radial depth is described by Fig. 7 and the axial depth is 5 mm. Note that the OPR samples appear as a black line for this time scale.

Figures 9-12 also include the once-per-revolution (OPR) samples from the time-domain simulation. These samples serve as a stability metric [35-36]. If the samples repeat during constant depth machining, this indicates forced vibration and stable cutting conditions. If they do not repeat during constant depth machining, this identifies self-excited vibration, or chatter. During variable radial depth machining, the transient nature of the signal means the OPR samples do not repeat. Stable cutting conditions are identified by the repeating OPR samples (circles) in Figs. 9-12. The variation in force amplitude from one tooth to the next in Figs. 11-12 is due to runout of the four teeth on the rotating endmill. The runout was measured using a dial indicator and included in the time-domain simulation.

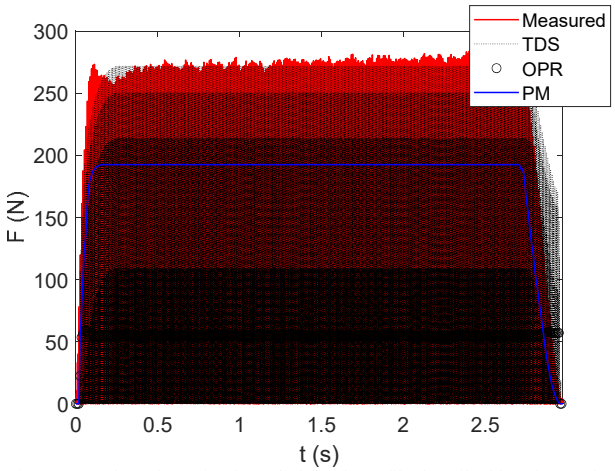

Fig. 10. Resultant force for the radial depth profile described by Fig. 7. The axial depth is 5 mm.

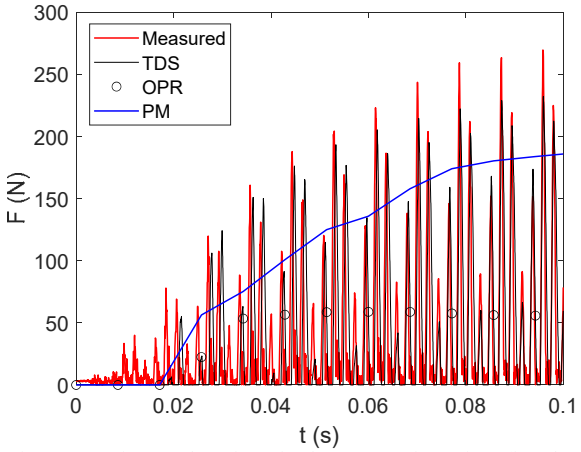

Fig. 11. Transient resultant force for the cut entry from Fig. 7 (i.e., the first 0.1 s in Fig. 10). The axial depth is 5 mm.

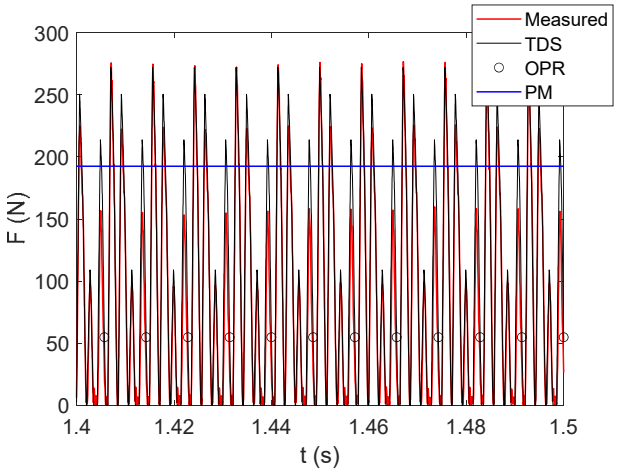

Fig. 12. Steady-state resultant force from Fig. 7 (i.e., 0.1 s starting at 1.4 s in Fig. 10). The axial depth is 5 mm.

Figures 13-14 mimic Figs. 11-12, but the radial depth is 6.35 mm (50% radial immersion) and the axial depth is 12 mm. Although the time scales are identical, the force levels are higher due to the increased depths of cut. The repeating OPR samples (circles) in Fig. 14 again indicate stable machining performance.

The final constant radial depth of cut case was performed with a radial depth of 12.7 mm (100% radial immersion) and axial depth of 12 mm; see Figs. 15 and 16. The selected depth of cut-spindle speed combination is unstable (chatter); this is demonstrated by the non-repeating OPR samples in Fig. 16. Note the large forces for the chatter conditions. The good agreement between the measured and time-domain simulation results validates the force model.

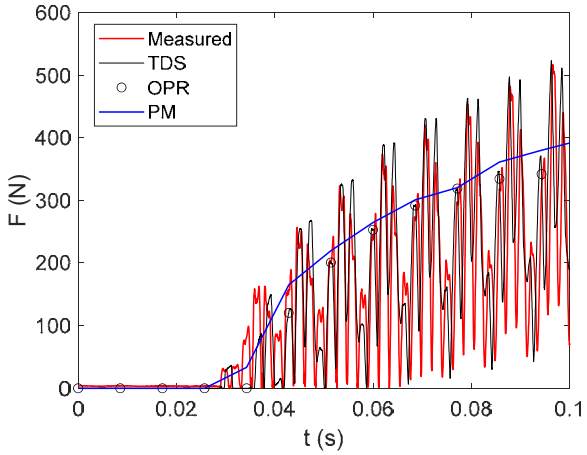

Fig. 13. Transient resultant force for radial depth of 6.35 mm and axial depth of 12 mm.

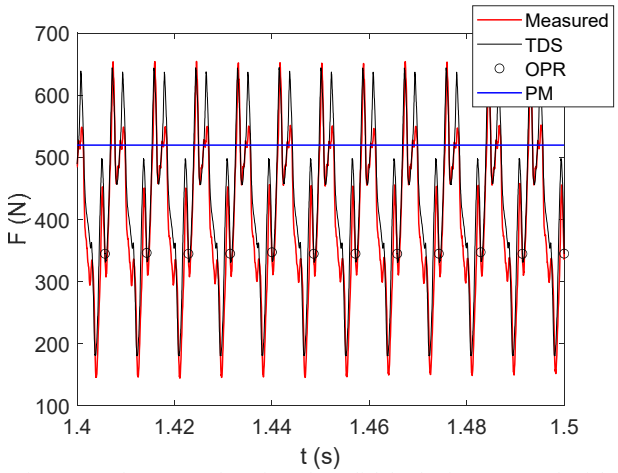

Fig. 14. Steady-state resultant force for radial depth of 6.35 mm and axial depth of 12 mm.

6.2. Ramp geometry – Variable radial depth

The machining setup described in Section 3.1 was again used to machine a 6061-T6 aluminum workpiece bolted to the Kistler 9257B cutting force dynamometer. The workpiece geometry was the ramp profile shown in Fig. 5 with the variation in radial depth displayed in Fig. 6. The radial depth of cut varied from 3.18 mm (25% radial immersion) to 12.7 mm (100% radial immersion) for the ramp profile and the axial depths were 3 mm to 12 mm over multiple cutting tests. The spindle speed was 7000 rpm and the feed per tooth was 0.05 mm. Flood coolant was applied to evacuate chips.

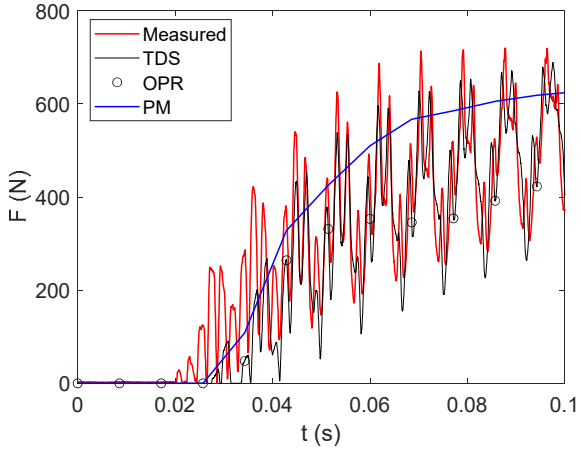

Fig. 15. Transient resultant force for radial depth of 12.7 mm and axial depth of 12 mm.

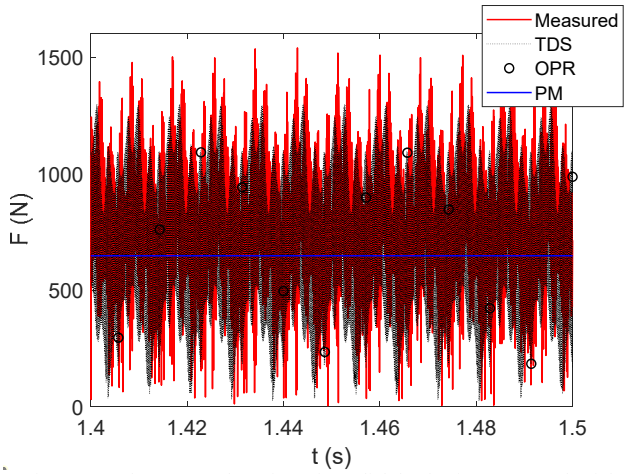

Fig. 16. Steady-state resultant force for radial depth of 12.7 mm and axial depth of 12 mm.

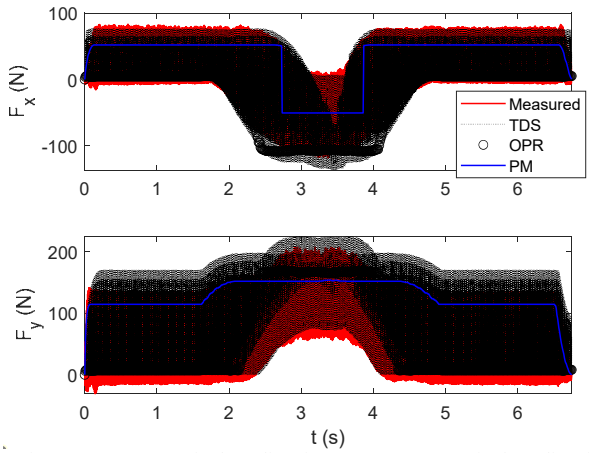

Fig. 17. (Top) Forces in the *x* direction. (Bottom) Forces in the *y* direction. The radial depth is described by Fig. 6 and the axial depth is 7 mm.

The ramp profile's radial depth variation (from Production Module) was input to the time-domain simulation, as well as the tool tip FRFs and force model, and the dynamic cutting forces in the *x* (feed) and *y* directions were calculated for an axial depth of 7 mm. Figure 17 shows the time-dependent *x* and *y* direction force components, Fig. 18 displays the resultant force, Fig. 19 shows the force variation during the cut entry, and Fig. 20 gives the force near the middle of the toolpath. Note that this force is nominally constant because the cutting force is constant for a four-tooth endmill under slotting conditions with no runout [15]. The repeated OPR samples in Fig. 20 show that the cut is stable and the TDS and measurement results agree.

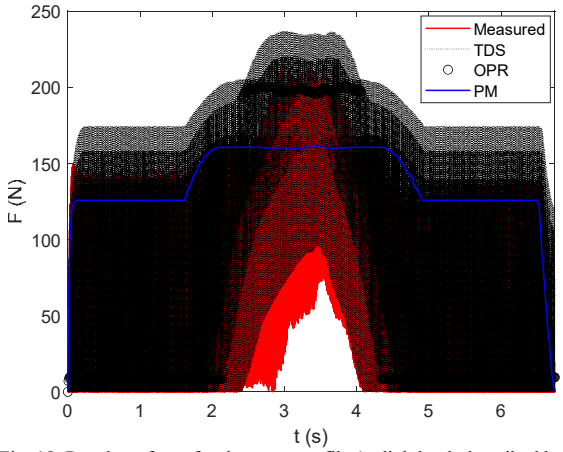

Fig. 18. Resultant force for the ramp profile (radial depth described by Fig. 6). The axial depth is 7 mm.

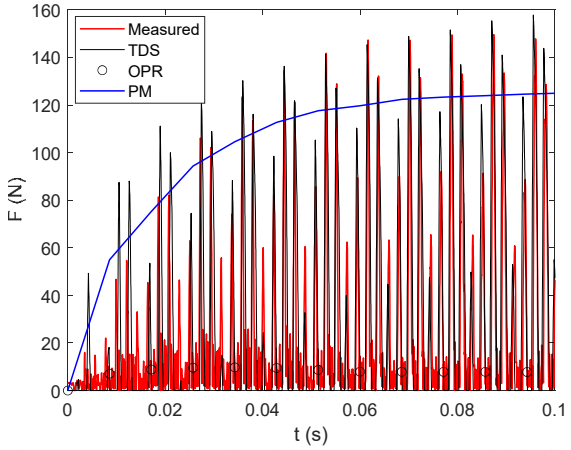

Fig. 19. Transient resultant force for ramp profile with an axial depth of 7 mm.

Figures 21-25 display results for the second ramp case. The axial depth is 12 mm and the cutting conditions are now unstable near the middle of the toolpath. It is observed that both the measured and TDS forces grow dramatically as the radial depth approaches 12.7 mm (slotting) and chatter occurs.

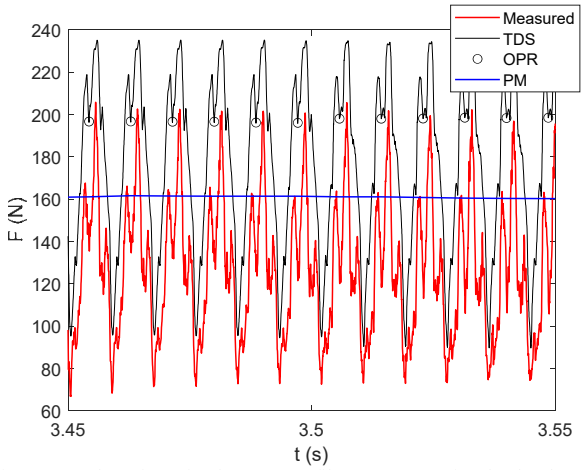

Fig. 20. Resultant force for the ramp profile near center of toolpath. The axial depth is 7 mm.

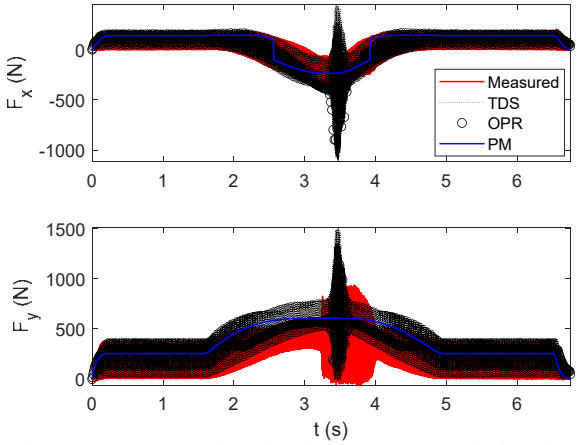

Fig. 21. (Top) Forces in the *x* direction. (Bottom) Forces in the *y* direction. The radial depth is described by Fig. 6 and the axial depth is 12 mm.

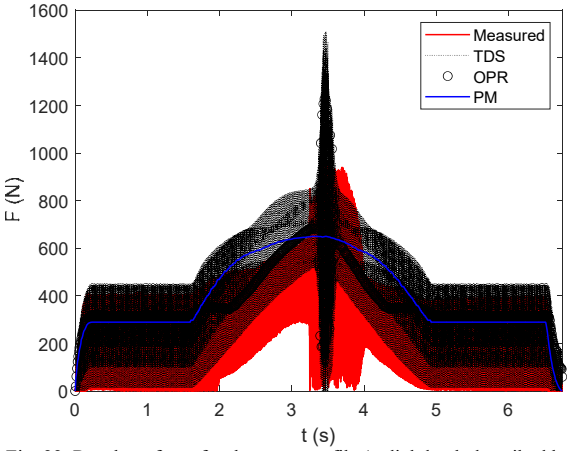

Fig. 22. Resultant force for the ramp profile (radial depth described by Fig. 6). The axial depth is 12 mm.

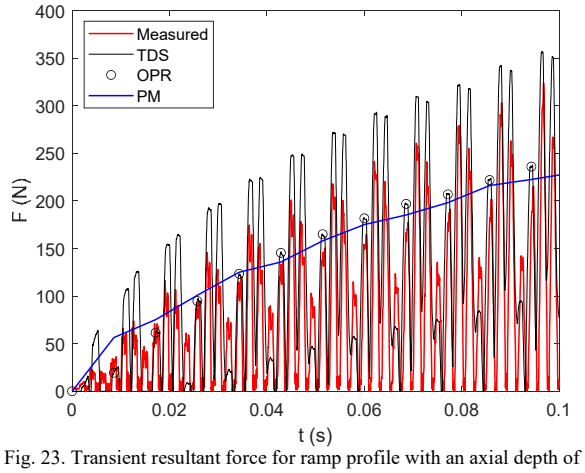

Fig. 23. Transient resultant force for ramp profile with an axial depth of 12 mm.

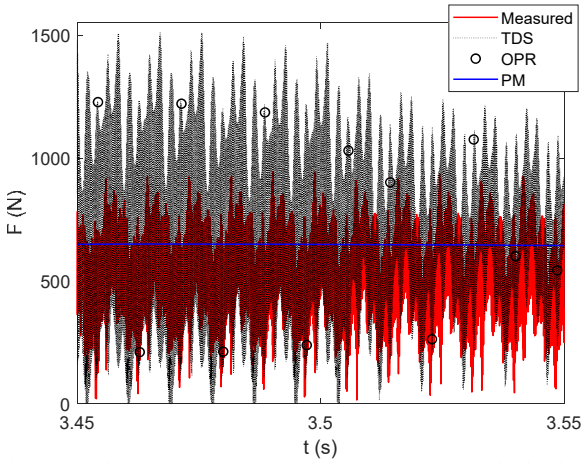

Fig. 24. Resultant force for the ramp profile near center of toolpath. The axial depth is 12 mm and chatter is observed.

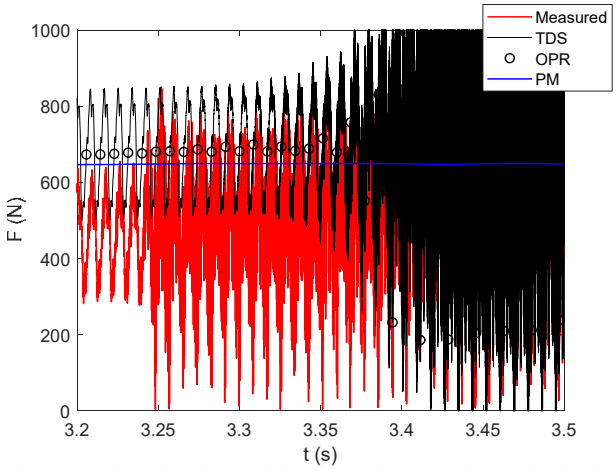

Fig. 25. Resultant force for transition from stable to unstable cutting for the ramp profile near center of toolpath. The axial depth is 12 mm.

Figure 25 displays the transition to chatter for both the measured and TDS resultant force. Although the transition does not occur at exactly the same time (and, therefore, radial depth), the behavior is similar. The force profile changes from the repeated revolution-to-revolution force to the self-excited vibration force profile that does not repeat and grows in amplitude.

7. Conclusions

This paper combined time-domain milling simulation and feed rate scheduling software to predict dynamic cutting force components. The time-domain simulation inputs included the tool tip frequency response functions, cutting force model, and instantaneous radial depth of cut. The radial depth of cut profiles were obtained from the feed rate scheduling software Production Module provided by Third Wave Systems. Two sets of machining trials were completed. First, constant radial depth of cut tests were completed to validate the force model and time-domain simulation force predictions against measurement. Both stable and unstable (chatter) milling conditions were observed with good agreement between time-domain simulation and measurement results. Comparisons to Production Module peak force predictions were also completed. The trends agreed for stable cutting conditions. Second, a ramp geometry tool path was selected with variable radial depth of cut. Comparisons between measurements and time-domain simulation were completed for both stable and unstable cutting conditions. The variable radial depth was again predicted by Production Module and was input to the time-domain simulation. Production Module peak force predictions trends agreed with measurement and time-domain simulation for stable cutting conditions. This effort demonstrates the value when including structural dynamics in cutting force predictions for machining optimization.

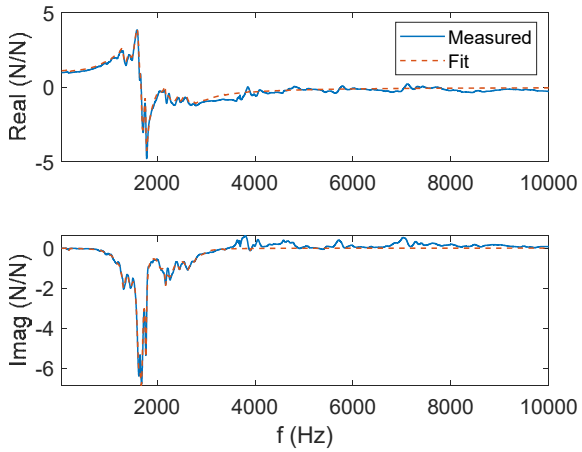

Fig. A1. Force-to-force FRF for *x* direction on Kistler 9257B dynamometer.

Appendix A: Inverse filtering

Because the Kistler 9257B dynamometer is a dynamic system, its dynamic response can affect the measured force depending on the force frequency content. To remove these effects, the force-to-force frequency response function (FRF) was measured using a PCB Piezotronics modal hammer (model number 086C04). The measured FRFs and modal fits are displayed in Fig. A1 (*x* direction) and Fig. A2 (*y* direction). These FRFs were then inverted and a low-pass filter (4500 Hz

cutoff frequency) was convolved; see Fig. A3 (x and y directions). The measured force components in the x and y directions were converted to the frequency domain using the Fourier transform and multiplied by the Fig. A3 filters. After conversion back to the time domain using the inverse Fourier transform, the filtered force was compared against the time-domain simulation and Production Module peak force values.

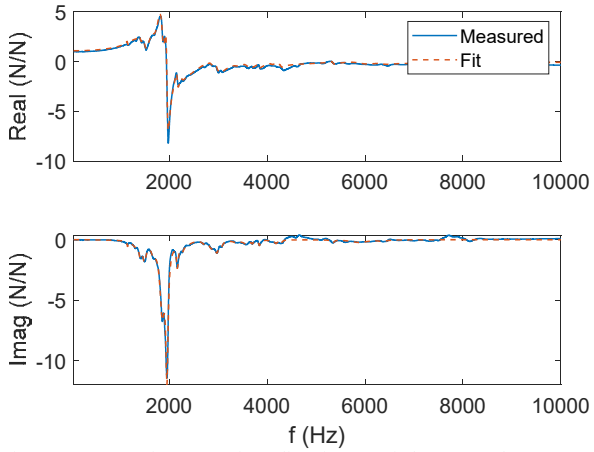

Fig. A2. Force-to-force FRF for y direction on Kistler 9257B dynamometer.

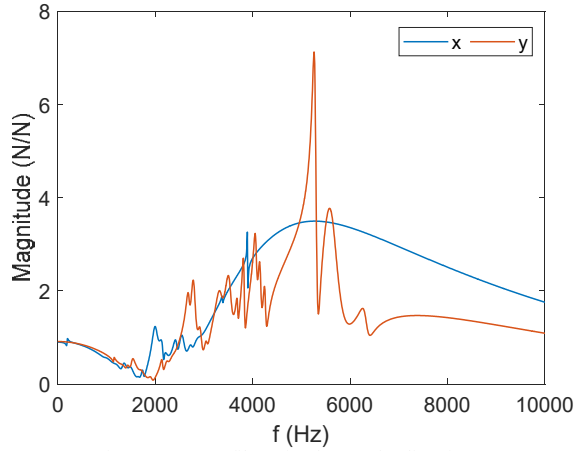

Fig. A3. Inverse filters for the x and y directions.

Acknowledgements

The authors gratefully acknowledge the use of the Production Module software from Third Wave Systems. This work was supported by the DOE Office of Energy Efficiency and Renewable Energy (EERE), Advanced Manufacturing Office (AMO), under contract DE-AC05-00OR22725. The US government retains and the publisher, by accepting the article for publication, acknowledges that the US government retains a nonexclusive, paid-up, irrevocable, worldwide license to publish or reproduce the published form of this manuscript, or allow others to do so, for US government purposes. DOE will provide public access to these results of federally sponsored research in accordance with the DOE Public Access Plan (http://energy.gov/downloads/doe-public-access-plan).

References

[1] Tobias, S.A., 1965. Machine-tool vibration. Blackie.
[2] Tlusty, J., 1986. Dynamics of high-speed milling. J. Eng. Ind., 108(2), pp.59-67.
[3] Altintaş, Y. and Budak, E., 1995. Analytical prediction of stability lobes in milling. CIRP annals, 44(1), pp.357-362.
[4] Merdol, S.D. and Altintas, Y., 2004. Multi frequency solution of chatter stability for low immersion milling. J. Manuf. Sci. Eng., 126(3), pp.459-466.
[5] Altintas, Y. and Weck, M., 2004. Chatter stability of metal cutting and grinding. CIRP annals, 53(2), pp.619-642.
[6] Schmitz, T.L. and Mann, B.P., 2006. Closed-form solutions for surface location error in milling. International Journal of Machine Tools and Manufacture, 46(12-13), pp.1369-1377.
[7] Mann, B.P., Edes, B.T., Easley, S.J., Young, K.A. and Ma, K., 2008. Chatter vibration and surface location error prediction for helical end mills. International Journal of Machine Tools and Manufacture, 48(3-4), pp.350-361.
[8] Kiran, K., Rubeo, M., Kayacan, M.C. and Schmitz, T., 2017. Two degree of freedom frequency domain surface location error prediction. Precision Engineering, 48, pp.234-242.
[9] Tlusty, J. and Ismail, F., 1981. Basic non-linearity in machining chatter. CIRP Annals, 30(1), pp.299-304.
[10] Tlusty, J., Zaton, W. and Ismail, F., 1983. Stability lobes in milling. CIRP Annals, 32(1), pp.309-313.
[11] Smith, S. and Tlusty, J., 1991. An overview of modeling and simulation of the milling process. Transactions of the ASME: Journal of Engineering for Industry, 113, pp.169-175
[12] Smith, S. and Tlusty, J., 1993. Efficient simulation programs for chatter in milling. CIRP annals, 42(1), pp.463-466.
[13] Schmitz, T. and Ziegert, J., 1999. Examination of surface location error due to phasing of cutter vibrations. Precision Engineering, 23(1), pp.51-62.
[14] Schmitz, T.L., Couey, J., Marsh, E., Mauntler, N. and Hughes, D., 2007. Runout effects in milling: Surface finish, surface location error, and stability. International Journal of Machine Tools and Manufacture, 47(5), pp.841-851.
[15] Schmitz, T. and Smith, K.S., 2009. Machining Dynamics: Frequency Response to Improved Productivity, Springer Science.
[16] Honeycutt, A. and Schmitz, T.L., 2017. Surface location error and surface roughness for period-n milling bifurcations. Journal of Manufacturing Science and Engineering, 139(6).
[17] Mann, B.P., Young, K.A., Schmitz, T.L. and Dilley, D.N., 2005. Simultaneous stability and surface location error predictions in milling. J. Manuf. Sci. Eng., 127(3), pp.446-453.
[18] Insperger, T., Gradišek, J., Kalveram, M., Stepan, G., Winert, K. and Govekar, E., 2006. Machine tool chatter and surface location error in milling processes. J. Manuf. Sci. Eng., 128(4), pp.913-920.
[19] Insperger, T. and Stépán, G., 2011. Semi-discretization for time-delay systems: Stability and engineering applications (Vol. 178). Springer Science & Business Media.
[20] Ding, Y., Zhu, L., Zhang, X. and Ding, H., 2011. On a numerical method for simultaneous prediction of stability and surface location error in low radial immersion milling. Journal of Dynamic Systems, Measurement, and Control, 133(2).
[21] Dong, J., Ferreira, P.M. and Stori, J.A., 2007. Feed-rate optimization with jerk constraints for generating minimum-time trajectories. International Journal of Machine Tools and Manufacture, 47(12-13), pp.1941-1955.
[22] Altintas, Y. and Erkorkmaz, K., 2003. Feedrate optimization for spline interpolation in high speed machine tools. CIRP Annals, 52(1), pp.297-302.
[23] Yazar, Z., Koch, K.F., Merrick, T. and Altan, T., 1994. Feed rate optimization based on cutting force calculations in 3-axis milling of dies and molds with sculptured surfaces. International Journal of Machine Tools and Manufacture, 34(3), pp.365-377.
[24] https://thirdwavesys.com/machining-modeling/productionmodule/.
[25] Lee, B.Y., Tarng, Y.S. and Ma, S.C., 1995. Modeling of the process damping force in chatter vibration. International Journal of Machine Tools and Manufacture, 35(7), pp.951-962.

[26] Huang, C.Y. and Wang, J.J., 2007. Mechanistic modeling of process damping in peripheral milling. J. Manuf. Sci. Eng., 129(1), pp.12-20.
[27] Rahnama, R., Sajjadi, M. and Park, S.S., 2009. Chatter suppression in micro end milling with process damping. Journal of Materials Processing Technology, 209(17), pp.5766-5776.
[28] Budak, E. and Tunc, L.T., 2010. Identification and modeling of process damping in turning and milling using a new approach. CIRP annals, 59(1), pp.403-408.
[29] Yusoff, A.R., Turner, S., Taylor, C.M. and Sims, N.D., 2010. The role of tool geometry in process damped milling. The International Journal of Advanced Manufacturing Technology, 50(9), pp.883-895.
[30] Sellmeier, V. and Denkena, B., 2012. High speed process damping in milling. CIRP Journal of Manufacturing Science and Technology, 5(1), pp.8-19.
[31] Ahmadi, K. and Ismail, F., 2012. Stability lobes in milling including process damping and utilizing multi-frequency and semi-discretization methods. International Journal of Machine Tools and Manufacture, 54, pp.46-54.
[32] Tunç, L.T. and Budak, E., 2013. Identification and modeling of process damping in milling. Journal of Manufacturing Science and Engineering, 135(2).
[33] Tyler, C. and Schmitz, T., 2013. Analytical process damping stability prediction. Journal of Manufacturing Processes, 15, pp.69-76.
[34] Tyler, C. and Schmitz, T., 2014. Process damping milling model database. Transactions of the NAMRI/SME, 42.
[35] Honeycutt, A. and Schmitz, T., 2017. Milling stability interrogation by subharmonic sampling, Journal of Manufacturing Science and Engineering, 139(4), pp.041009.
[36] Honeycutt, A. and Schmitz, T., 2016. A new metric for automated stability identification in time domain milling simulation. Journal of Manufacturing Science and Engineering, 138(7) pp.074501.